

Constraining the size of the Comptonizing medium by modeling the energy dependent time-lags of kHz QPOs of Neutron star system

Nagendra Kumar^{1*} and Ranjeev Misra^{1 †}

¹*Inter-University Centre For Astronomy and Astrophysics, Post Bag4, Ganeshkind, Pune-411007, India*

ABSTRACT

In earlier works, we had shown that the observed soft lags and r.m.s versus energy of the lower kHz QPO of neutron star binaries can be explained in the framework of a thermal Comptonization model. It was also shown that such an interpretation can provide estimates of the size and geometry of the Comptonizing medium. Here we study the dependence of these estimates on the time-averaged spectral model assumed and on the frequency of the QPO. We use the high quality time lag and r.m.s obtained during March 3rd 1996 observation of 4U 1608-52 by RXTE as well as other observations of the source at different QPO frequencies where a single time-lag between two broad energy bands have been reported. We compare the results obtained when assuming that the time-averaged spectra are represented by the spectrally degenerate “hot” and “cold” seed photon spectral models. We find that for the “hot” seed photon model the medium size is in the range of 0.3-2.0 kms and the size decreases with increasing QPO frequency. On the other hand for the “cold” seed photon model the range for the sizes are much larger 0.5-20 kms and hence perhaps show no variation with QPO frequency. Our results emphasize the need for broad band spectral information combined with high frequency timing to lift this degeneracy. We further show that the r.m.s as a function of energy for the upper kHz QPO is similar to the lower one and indeed we find that the driver for this QPO should be temperature variations of the corona identical to the lower kHz QPO. However, the time lag reported for the upper kHz QPO is hard, which if confirmed, would challenge the simple Comptonization model presented here. It would perhaps imply that reverberation lags are also important and/or the dominant spectral component is not a single temperature medium but a multi-temperature complex one.

Key words: radiation mechanisms: thermal-stars: neutron-X-rays: binaries-X-rays: individual: 4U 1608-52

1 INTRODUCTION

In neutron star low-mass X-ray binaries (LMXBs) systems, the neutron star accretes matter via Roche lobe overflow from a normal low-mass companion star. This accretion forms a disk and it is believed that the intense X-ray emissions arise from such an accretion disk. The X-rays can be emitted from the inner accretion disk and/or the boundary layer between the neutron star surface and the disk. These LMXBs are, in general, weakly magnetised, non-pulsating systems and are broadly divided phenomenologically into two sub-classes depending upon their long term X-ray luminosity variations. Some sources are considered to be ‘transient’ if their luminosities changes by more than 100 times while other are considered ‘persistent’ if their luminosities varies by factors of $\sim 2-10$ and if they have always been detectable over the history of X-ray astronomy (Psaltis 2006). Further, they are divided into two classes ‘Z’, and ‘atoll’, based on the correlation between their X-ray spec-

tral and timing properties (Hasinger & van der Klis 1989). In the color-color diagrams (CCDs), the Z sources trace out a roughly Z-shaped track within hours/day. The track of atoll sources in the CCD are generally C-shaped and the source covers the track on time scales of days to years. In general, all Z sources are persistent while atoll sources can be either persistent or transient. However, the classification may depend only on the luminosity since XTE J1701-462 shows characteristics of both atoll and Z sources depending on its flux level (Lin, Remillard & Homan 2009; Homan et al. 2010).

Quasi-periodic oscillations (QPO) in the frequency range, 400 – 1300 Hz have been discovered in most neutron star LMXBs with the Rossi X-ray Timing Explorer (RXTE) satellite (van der Klis 2006). Often two simultaneous kHz QPO are observed with their frequency separation ranging from ~ 200 to ~ 400 Hz and with their frequencies correlated with each other (Belloni, Mendez & Homan 2005, 2007). The QPO with the higher frequency is referred to as the “upper” kHz QPO while the other is called the “lower” kHz QPO.

A number of models have been proposed to physically in-

* E-mail: nagendrak@iucaa.in

† E-mail: rmisra@iucaa.in

interpret these twin kHz QPOs. Some of these models are: the sonic-point model (Miller, Lamb & Psaltis 1998; Lamb & Miller 2003); the relativistic precession model (Stella & Vietri 1999); the two-oscillator model (Osherovich & Titarchuk 1999; Titarchuk 2003); the relativistic resonant model (Kluźniak & Abramowicz 2001); deformed-disk oscillation model (Kato 2009; Mukhopadhyay 2009)); and magneto-hydrodynamic (MHD) models (Zhang 2004; Li & Zhang 2005; Shi & Li 2009; Erkut, Psaltis & Alpar 2008). A particular model is favoured if it can describe the correlation between the kHz frequencies with the properties of the lower frequency QPOs (10 – 200 Hz) which are also observed in these sources (e.g. Straaten, van der Klis & Mendez 2003; Altamirano et al. 2008). A model may also need to explain the conditions which determine the appearance of twin versus a single kHz QPO (e.g. Sanna et al. 2012; Lin et al. 2012; Mendez et al. 1998b). Unfortunately, there is no consensus on which among these is the most likely model (e.g. Lin, et al. 2011; Wang et al. 2013).

In this scenario, it maybe more prudent to understand the relation between the kHz QPOs and the X-ray flux and spectra and to identify the radiative process responsible for the QPOs irrespective of their dynamical origin. The frequencies of the kHz QPOs exhibit complex correlation with intensity. In short time-scales of hours they are positively correlated (Yu et al. 1997; Ford et al. 2000), while on longer time-scales they exhibit parallel tracks in the kHz QPO frequency versus intensity diagram (Mendez et al. 1999). The incidence of kHz QPOs also depends on the X-ray intensity (Misra & Shanthi 2004). The frequencies depend on the position of the source in the color-color diagram and two different tracks are traced out by the higher and lower kHz QPOs. Whenever a single kHz QPO is observed, it follow either the upper or lower kHz QPOs track (Mendez & van der Klis 1999; van der Klis 2000). In general, the occurrence of kHz QPOs on different positions of CCDs indicates that as the QPO frequency decreases, the X-ray spectrum tends to be harder, i.e., its hard color increases (Straaten, van der Klis & Mendez 2003; Altamirano et al. 2008; Lin et al. 2012).

The fractional root mean square (r.m.s.) amplitude of the kHz QPOs usually increases with photons energy at least up to 20 keV (Berger, et.al. 1996; Zhang et al. 1996; Wijnands et al. 1997b; van der Klis 2006). Beyond 20 keV the dependence is unknown with some indications that it may decrease (Mukherjee & Bhattacharyya 2012). In general, the strength of lower kHz QPOs is larger than the upper one at any energy bin (Mendez et al. 1998a; Wijnands et al. 1997a). Another important characteristic is the energy dependent time-lag shown by these QPOs. It was found that the ~ 18 keV photons have a time lag of $\sim -50\mu\text{s}$ with respect to the ~ 5 keV photons in the ~ 850 Hz lower kHz QPO in 4U 1608-52, the soft photon came later and hence these lags are referred to as “soft lag”. The soft lag associated with the lower kHz QPO was also found for another source 4U 1636-53 (Vaughan et al. 1997; Kaaret et al. 1999). Recently Peille et al. (2015), Barret (2013), and de Avellar et al. (2013) have confirmed the soft lag in lower kHz QPOs by analysing a large number of observations and found that the magnitude of the time-lags have a complex dependence on the QPO frequency. Moreover, de Avellar et al. (2013) claimed that the time lag of the lower and the upper kHz QPOs have opposite signs, i.e., the upper kHz QPOs exhibit hard lags.

The time averaged X-ray spectral modelling of NS LMXBs reveal that in these system, the inner region is partially or fully covered by a corona consisting of hot thermal electrons which Compton upscatter low energy photons. There are two types of phenomenological spectral models which are used to describe the X-ray emission in NS LMXBs. Both models describe the X-ray spec-

trum as sum of a soft black body like component and the other a harder component due to thermal Comptonization. In one model, the thermal component is interpreted as a multicolor disk black body (MCD) emission attributed to accretion disk, while the seed photons for the Comptonized component are emitted from close to the NS surface or the boundary layer (Mitsuda et al. 1984, 1989). In the other model (White et al. 1986), the soft component is a single temperature black body emission from the boundary layer, while the seed photons for the Comptonization are emitted from the accretion disk (see for e.g. Barret 2001; Di Salvo & Stella 2002; Paizis et al. 2006, for reviews of LMXBs X-ray spectral models). These two approaches of modelling are often degenerate i.e. they give equally statistically acceptable fit to data. Apart from the theoretical differences the critical radiative spectral difference between the two models is that in one the temperature of the direct soft component spectrum is lower (e.g. Gierlinski, & Done 2002; Tarana, Bazzano & Ubertini 2008; Agrawal & Misra 2009; Raichur, Misra & Dewangan 2011; Barret 2013) and in the other higher (e.g. Agrawal & Sreekumar 2003; Paizis et al. 2005; Farinelli, Titarchuk & Frontera 2007; Farinelli et al. 2008) than that of the seed photon source temperature of the thermal Comptonization. Thus in this work, following Lin, Remillard & Homan (2007), we refer to the former spectral model as “hot-seed model” and the latter model as “cold-seed model”. The typical spectral parameter values varies depending on the spectral state and in general, from the soft to the hard state, the temperature of corona ranges from ~ 2 keV to ~ 20 keV and the optical depth, τ_o ranges from ~ 10 to ~ 2 .

Energy dependent r.m.s and time lags of the kHz QPOs provide information on the spectral parameter whose variation is responsible for the phenomenon and can constrain the size and geometry of the system (Lee, & Miller 1998). This is also true for other lower frequency temporal behaviour as for example, in black hole X-ray binary system, the positive correlation between the fractional r.m.s. and photons energy has been explained due to corona temperature oscillation (Gierlinski & Zdziarski 2005). For thermal Comptonization, since the higher energy photons scatter more than the soft ones, it is expected that the system should show hard lag which is contradictory to the observations of kHz QPOs. However, Lee, Misra & Taam (2001) have shown that a system will show soft lags if some fraction of the Comptonized photons impinge back to the input source. There could also be time-lags introduced due to reflection of the X-rays from an accretion disk (Barret 2013).

In Kumar & Misra (2014) (hereafter Paper I) we studied the expected time lag due to thermal Comptonization by solving the linearised time dependent Kompaneets equation for different physical situations such as the primary oscillation being in the soft photon source or in the heating rate of the corona. We then compared the results with the RXTE observations of 4U 1608-52 on 3 March 1996 and concluded that the model can explain the data and inferred the corona’s size to be 0.3–2 km. The results depend on the steady state spectral parameters and there we had used a particular fitting of the data. However, as mentioned above, the spectral parameters of LMXBs in general are typically degenerate and it is important to check the differences obtained when one uses the cold-seed photon model or the hot-seed photon one. Moreover, the results of Barret (2013) and de Avellar et al. (2013) allow us to compare the model predictions for different kHz QPO frequencies and hence possibly infer the size and geometry as a function of frequency. Such a study will be useful to constrain hydrodynamical models which relate the size of the corona to the kHz QPO

frequency such as those given by Pal & Chakrabarti (2014) and Cabanac et al. (2010).

In the next section we briefly review the model using the linearised time dependent Kompaneets equation which is extensively described in Paper 1. In §3, we compare the model predictions for the low frequency kHz QPO observed in 4U 1608-52 on 3rd March 1996 considering both the soft and hot seed photon spectral models. In §4 we discuss the implication of the model on the high frequency kHz QPO. In §5 we try to constrain the size and geometry of the system for different frequencies, while in §6 we summarise and discuss the results.

2 VARIABILITY OF THERMAL COMPTONIZED PHOTONS

In the non-relativistic limit (i.e. $kT_e \ll m_e c^2$) and for low photon energies ($E \ll m_e c^2$), the evolution of the photon density (n_γ) inside a Comptonizing medium is governed by the Kompaneets equation (Kompaneets 1957),

$$t_c \frac{dn_\gamma}{dt} = \frac{1}{m_e c^2} \frac{d}{dE} \left[-4kT_e E n_\gamma + E^2 n_\gamma + kT_e \frac{d}{dE} (E^2 n_\gamma) \right] + t_c \dot{n}_{s\gamma} - t_c \dot{n}_{esc} \quad (1)$$

where the induced scattering term has been neglected and the equation is written in terms of the photon density rather than photon occupation number. Here

$$\dot{n}_{s\gamma} = \left[\frac{4\pi a^2}{V_c} \right] \left(\frac{2\pi}{h^3 c^2} \frac{E^2}{\left(\exp \left[\frac{E}{kT_b} \right] - 1 \right)} \right) \quad (2)$$

is the rate of input photons per unit volume. A simplified geometry has been assumed in which a spherical black body seed photon source at a temperature T_b and radius a is surrounded by a corona of width L and temperature T_e . Thus, the Comptonizing medium has a volume $V_c = (4/3)\pi[(a+L)^3 - a^3]$, the Thompson collision time scale $t_c = 1/(cn_e\sigma_T)$, and the optical depth of medium $\tau = \frac{(L/c)}{t_c}$, where σ_T is the Thompson cross-section and n_e is the electron density. The escape rate of the photon density is taken to be $\dot{n}_{esc} \simeq \frac{n_\gamma}{(\tau^2 + \tau)t_c}$, where $(\tau^2 + \tau)$ is assumed to be the average number of scatterings. The emergent X-ray spectrum is determined by \dot{n}_{esc} in steady state (i.e., $\frac{dn_\gamma}{dt} = 0$) where $n_{\gamma o}$ is computed for corresponding steady state (or time-averaged) values of T_{eo} and T_{bo} and τ .

The corona temperature reaches a steady state when the external heating rate per electron (\dot{H}_{Ex} , although its nature is unknown) is balanced by the Compton cooling rate per electron ($\langle \dot{\Delta E} \rangle = \int_{E_{min}}^{E_{max}} (4kT_e - E) \frac{E}{m_e c^2} n_\gamma \sigma_T c dE$). In general the time evolution of corona temperature is described as :

$$\frac{3}{2} k \frac{\partial T_e}{\partial t} = \dot{H}_{Ex} - \langle \dot{\Delta E} \rangle \quad (3)$$

The soft photon source has an internal heating rate which is taken to be $4\pi a^2 \sigma (T_b')^4$, such that in the absence of any another heating it temperature would be T_b' . Since we consider the possibility that a fraction η , of the Comptonized photons impinge back onto the seed photon source, the actual temperature T_b is given by,

$$4\pi a^2 \sigma T_b^4 = 4\pi a^2 \sigma T_b'^4 + \eta V_c \int \frac{n_\gamma}{(\tau^2 + \tau)t_c} E dE \quad (4)$$

For a given value of T_b , there is a maximum allowable value of η ,

η_{max} for which T_{bo}' is zero. The variation in \dot{H}_{Ex} will lead to variation in T_e while T_b can be varied from its steady state value due to fluctuations in the back-scattered photons. If their variability amplitude is small, the time averaged X-ray spectrum will correspond to the steady parameters, T_{eo} , τ and T_{bo} .

The energy dependent temporal features are assumed to be driven by fluctuation of the medium temperature and/or the source photon temperature over their averaged values i.e. $T_e = T_{eo}(1 + \Delta T_e e^{-i\omega t})$, or $T_b = T_{bo}(1 + \Delta T_b e^{-i\omega t})$. Here, ω is the angular frequency of the oscillation and their oscillation amplitude $\Delta T_e \ll 1$ and $\Delta T_b \ll 1$ are in general complex quantities. These fluctuation will lead to variation in photon density $n_\gamma = n_{\gamma o}(1 + \Delta n_\gamma e^{-i\omega t})$ and its amplitude Δn_γ is computed using the linearised Kompaneets equation (e.g. Lee, & Miller 1998; Lee, Misra & Taam 2001):

$$-\frac{d^2 \Delta n_\gamma}{dE^2} + \left(\frac{-1}{kT_{eo}} - \frac{2}{n_{\gamma o}} \frac{dn_{\gamma o}}{dE} \right) \frac{d\Delta n_\gamma}{dE} + \frac{m_e c^2 t_c (\dot{n}_{s\gamma o} - i\omega n_{\gamma o})}{E^2 n_{\gamma o} k T_{eo}} \Delta n_\gamma = \left(\frac{-2}{E^2} + \frac{1}{n_{\gamma o}} \frac{d^2 n_{\gamma o}}{dE^2} \right) \Delta T_e + \frac{m_e c^2 t_c \dot{n}_{s\gamma o}}{E^2 n_{\gamma o} k T_{eo}} \left(\frac{\frac{E}{kT_{bo}}}{1 - \exp\left(\frac{-E}{kT_{bo}}\right)} \right) \Delta T_b \quad (5)$$

$\Delta n_\gamma(E)$ determines the energy dependent temporal features. In particular $|\Delta n_\gamma(E)|$ is the fractional r.m.s, and the argument of $[\Delta n_\gamma(E_1)\Delta n_\gamma^*(E_2)]$ is the phase lag between two energies E_1 and E_2 . The mean phase lag between two energy band (say, (E_{1toE_2}) & (E_{3toE_4})) is the argument of $[\Delta n_\gamma(E_{12})\Delta n_\gamma^*(E_{34})]$, where $\Delta n_\gamma(E_{ab}) = \frac{\int_{E_a}^{E_b} n_{\gamma o} \Delta n_\gamma dE}{\int_{E_a}^{E_b} n_{\gamma o} dE}$.

Two possible cases are considered which can drive the temporal features of X-ray spectrum. In one case, the primary variation is that of the seed photon temperature leading to variations of the photon density. This in turn will lead to a variation in the corona temperature given by linearising Eqn. (3) i.e.

$$\frac{3}{2} k T_{eo} \Delta T_e (i\omega) = \frac{\sigma_T c}{m_e c^2} \left[\int 4kT_{eo} (\Delta T_e + \Delta n_\gamma) n_{\gamma o} E dE - \int E^2 \Delta n_\gamma n_{\gamma o} dE \right] \quad (6)$$

where the heating rate of the corona has been assumed to be a constant.

In the other case, the primary variation is that of the coronal heating rate, i.e. $\dot{H}_{Ex} = \dot{H}_{Exo}(1 + \Delta \dot{H}_{Ex} e^{-i\omega t})$, which will lead to the variation in the corona temperature and its amplitude is computed as:

$$\frac{3}{2} k T_{eo} \Delta T_e (-i\omega) = \dot{H}_{Exo} \Delta \dot{H}_{Ex} - \frac{\sigma_T c}{m_e c^2} \left[\int 4kT_{eo} (\Delta T_e + \Delta n_\gamma) n_{\gamma o} E dE - \int E^2 \Delta n_\gamma n_{\gamma o} dE \right] \quad (7)$$

which is the linearised form of Eqn (3). The seed photon temperature will fluctuate as response to the fluctuation in T_e and its amplitude ΔT_b is computed by linearising the Eqn. (4) as:

$$4\sigma (T_{bo})^4 \Delta T_b = \frac{\eta V_c}{4\pi a^2} \int \frac{n_{\gamma o}}{(\tau^2 + \tau)t_c} \Delta n_\gamma E dE \quad (8)$$

In both cases, the fluctuation of T_b or T_e are coupled to each other. In particular, their coupled amplitudes ΔT_e & ΔT_b are obtained by solving two complex equations (5), (6) or (5), (8) simultaneously in an iterative manner.

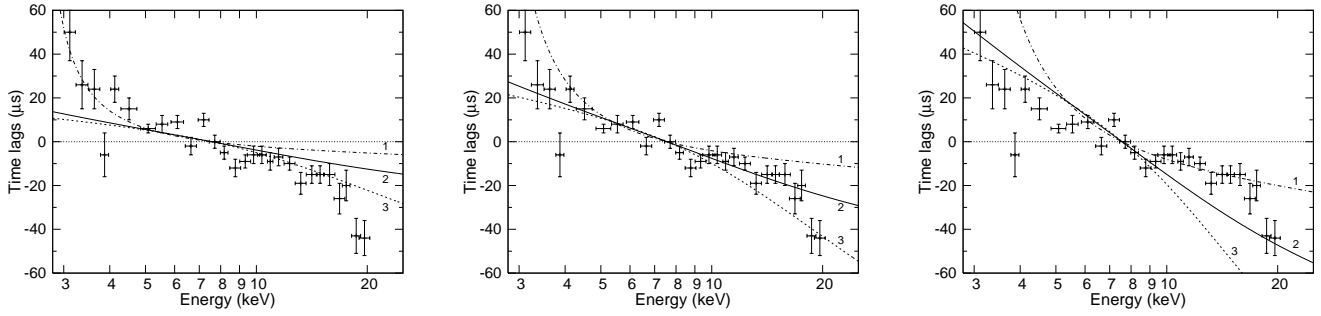


Figure 1. Time lags versus energy for the 3-March-1996 observation of 4U 1608-52 when the time-averaged spectral model is the ‘hot’ seed photon one. The left, middle and right panels are for $L = 0.25, 0.50,$ and 1.0 km respectively and the curves marked 1, 2, and 3 are for $\eta = 0.35, 0.55,$ and 0.65 respectively. The best description of data is obtained for $L = 0.5$ km and $\eta = 0.55$ (solid line in the middle panel).

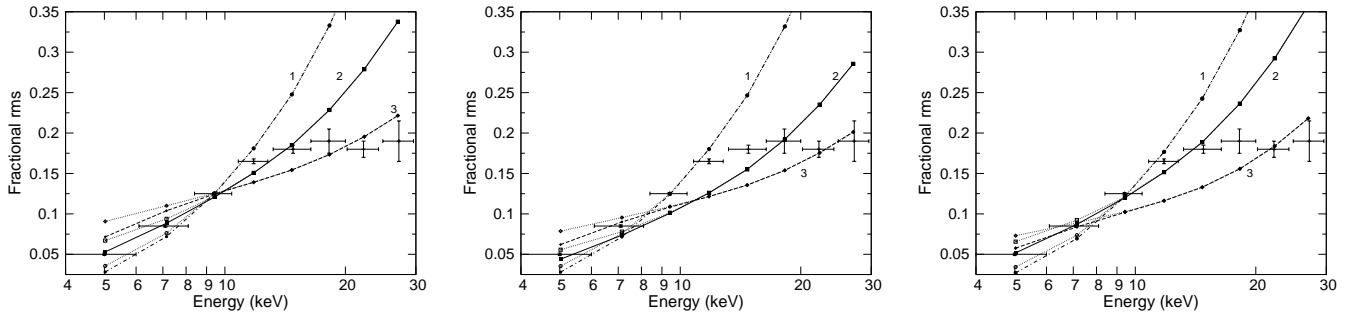


Figure 2. Fractional rms versus energy for the 3-March-1996 observation of 4U 1608-52 when the time-averaged spectral model is the ‘hot’ seed photon one. The predicted lines correspond to the same parameters as used for the lines in Figure 1. The solid points refer to the r.m.s of the main thermal Comptonization component. The open circles are the corrected r.m.s values when the constant contributions of other components such as the soft thermal component and the Iron line is taken into account.

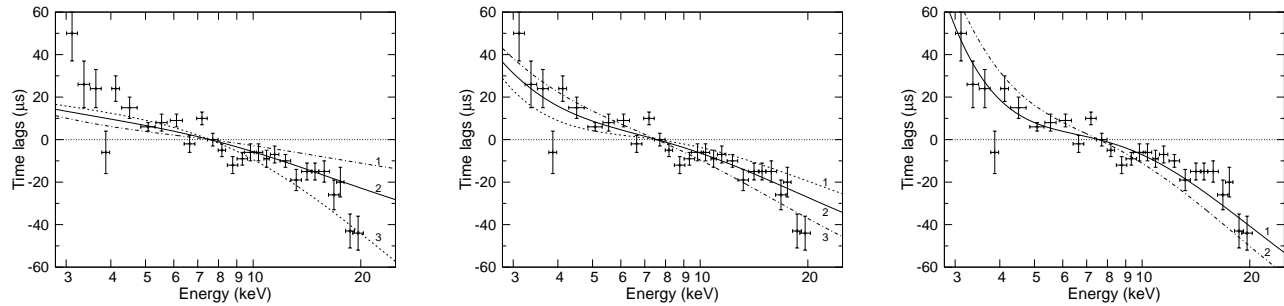


Figure 3. Time lags versus energy for the 3-March-1996 observation of 4U 1608-52 when the time-averaged spectral model is the ‘cold’ seed photon one. The left panel is for $L=0.5$ km and the curves marked 1, 2, and 3 are for $\eta = 0.3, 0.4,$ and 0.47 respectively. The middle panel is for $L = 2$ km and the curves marked 1, 2, and 3 are for $\eta = 0.20, 0.25,$ and 0.3 respectively. The right panel is for $L = 5$ km and the curves marked 1 and 2 are for $\eta = 0.25$ and 0.3 respectively. The best description of data is obtained for $L = 2$ km and $\eta = 0.25$ (solid line in the middle panel).

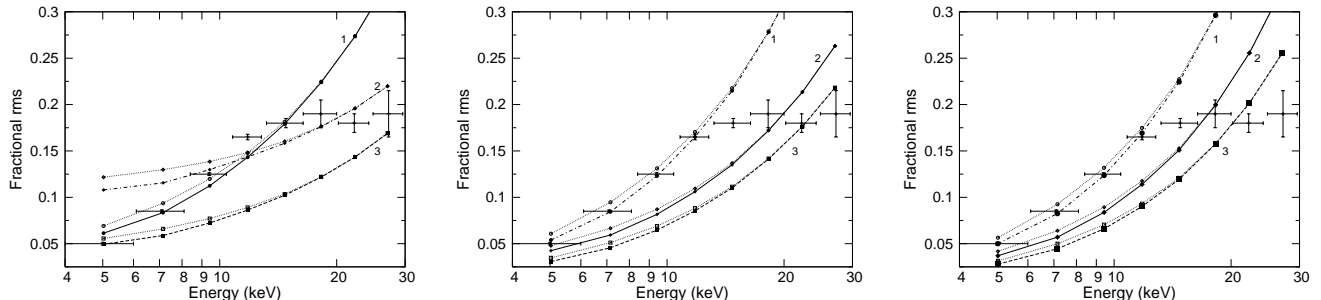


Figure 4. Fractional rms versus energy for the 3-March-1996 observation of 4U 1608-52 when the time-averaged spectral model is the ‘cold’ seed photon one. The predicted lines correspond to the same parameters as used for the lines in Figure 3 and the points have same meaning as Figure 2.

3 Comparison of X-ray spectral model with energy dependent temporal properties of 4U 1608-52

The RXTE observation of the ~ 850 Hz QPO of 4U 1608-52 on 3rd March 1996, remains one of the best cases for the energy dependent study of kHz QPOs. Berger, et.al. (1996) studied the energy depended fractional r.m.s for this observation, while Kaaret et al. (1999) and Vaughan et al. (1997) had shown that the lower kHz QPO exhibits soft lag. Recently Barret (2013) have computed the lag versus energy for a larger number of energy bins. In Paper I, we have shown that if the oscillation is due to the soft photon source, the time lags are always hard. However, when the medium temperature is the driver of the oscillation, the time lags are soft when a significant fraction of the Comptonized photons impinge back into the seed photon source. Indeed, the qualitative features of the time lag and r.m.s versus energy were reproduced by the model and a size of the corona was estimated for a particular set of spectral parameters. However, as described in the Introduction, in general, the spectra of LMXBs can be fitted by two spectrally degenerate models, the hot and cold seed photon models, and here we study the dependence of the time-lag and r.m.s on using these models.

Barret (2013) analysed the spectrum during the 3 March 1996 observation and used a model consisting of a disk black body, a thermal Comptonization component and an Iron emission line. The spectral parameters obtained of the Comptonization component were $kT_e = 2.69$ keV, optical depth $\tau^2 = 38.9$ and soft photon temperature of 1.02 keV. It was these spectral parameters that we used in Paper I to estimate the predicted time lag and r.m.s as a function of energy. For clarity, we reproduce here the same results in Figures 1 and 2. The left, middle and right figures are for different values of the size of the system while the curves drawn are for different values of the fraction impinging back to the soft source, η . The curves shown in the left and right panels of Figure 1 which are for a size of 0.25 and 1 kms respectively, do not match the observed points, while the curve in the middle panel for a size of 0.5 kms predicts the observed values. Hence, from these Figures one can deduce that for this spectral model, the size of the corona should be around 0.5 kms and $\eta \sim 0.5$. The spectral model used by Barret (2013) represents the hot-seed photon model since the seed photon temperature is high, i.e. ~ 1 keV.

In the literature, we did not find spectral analysis of this observation for the cold-seed photon model. Hence, we performed the spectral analysis of the data using a model consisting of a black body, a Comptonized component and an Iron line, all modified by absorption. The fitting was done using the XSPEC package where the model was described by wabs*(BB+CompTT+Gauss). The hydrogen column density for the interstellar absorption was fixed at $N_H = 1.5 \times 10^{22} \text{ cm}^{-2}$ (Barret 2013) and the intrinsic width of Gaussian line was fixed to 0.1 keV (Lin, Remillard & Homan 2007). The best fitted spectral parameter for the Comptonized component were 2.66 keV, 40.4 and 0.4 keV for electron temperature (kT_e), optical depth (τ^2), and seed photons temperature (kT_b) respectively. The low value of the seed photon temperature implies that this model belongs to the cold-seed photon family. Our motivation here is not to describe the spectrum accurately, but rather to understand the effect of the different spectra on the r.m.s and time lags of the kHz QPO. Figures 3 and 4 compare the observed time-lag and r.m.s with the predicted values for the cold-seed model. For both the cold and hot-seed models, there is a range of size and η that broadly explains the time lag and r.m.s dependence on energy and hence the temporal behaviour cannot distinguish between the two. However, the range of allowed values, especially for the size

of the system, depends on the model used. In the hot-seed model the allowed range of L size is from 0.25 to 1 km, while for the cold-seed model the allowed range is 0.5 to 5 km.

There are a couple of points highlighted in Paper I, which need to be re-emphasised here. The model generally over predicts r.m.s values at high energy which is also true when the spectral model is the cold-seed one. This suggests the possibility that there may be an additional non varying high energy component. The other point is that there are known additional components like the soft component (which is modelled as either a black body or disk black body remission) and the Iron line feature. However, these components if assumed not to be varying at the kHz frequency, do not have much effect on the energy dependence of the r.m.s. This is demonstrated in Figures 2 and 4 where the filled circles represent when the r.m.s is corrected for these components while the open circles are when it is not.

While we compare the predictions with the observed data, a formal fitting of the data has not been attempted. This is because of the several assumptions such as the geometry of the system and neglect of additional time delay due to reprocessing. However, we mention in passing that it seems the modelling prefers the hot-seed model by providing perhaps a more realistic size for the corona and that it seems to provide a “better” fit to the energy dependent time lag than the cold-seed photon one (compare the solid line in the middle panels of Figures 1 and 3).

4 Possible Driver for upper kHz QPOs in 4U 1608-52

For the same 3-March-1996 observation of 4U 1608-52, Mendez et al. (1998a) reported the detection of a simultaneous upper kHz QPO at ~ 1050 Hz and have computed the fractional r.m.s as a function of energy till about ~ 20 keV. Later by averaging several data sets, Mendez, van der Klis, & Ford (2001) present the fractional r.m.s for the upper kHz QPO and we consider the r.m.s. for energies > 20 keV from this averaged analysis. There are no reported measure of the energy dependent time-lag for the upper kHz QPO for the 3-March observations and hence we consider the time-lag computed by de Avellar et al. (2013) obtained by averaging several observations.

Since the lower and upper kHz QPOs are observed simultaneously, the geometry of the system and the time-averaged spectral parameters should be naturally same for both QPOs. If like the lower kHz QPO, the upper one is also driven by variations in the medium temperature, then the nature of the r.m.s and time-lag behaviours should be similar for both of them. In particular the expected time-lag should be soft. However this seems to contradict the results obtained by de Avellar et al. (2013) where the time-lag for the upper kHz QPO was reported to be hard or qualitatively different than those of the lower kHz QPO. This suggests that the perhaps the driving mechanism for the two QPOs is different. Indeed, as we had reported in Paper I, if the QPO is driven by variation in the soft photons source, the time-lag is expected to be always hard. However, as can be seen in Figure 5, the r.m.s versus energy data points are similar to the lower kHz QPO in the sense that the r.m.s increases with energy. On the other hand, as shown in Paper I, if a QPO is driven by the soft photon source the r.m.s behaviour is different and has a pivot point. Thus, when we try to fit the r.m.s of the upper QPO using such a model as shown in the left panel of Figure 5 we always find a pivot point at ~ 10 keV which is not seen in the data. In contrast, when we consider fluctuations in the corona temperature either the hot or cold seed model (middle and

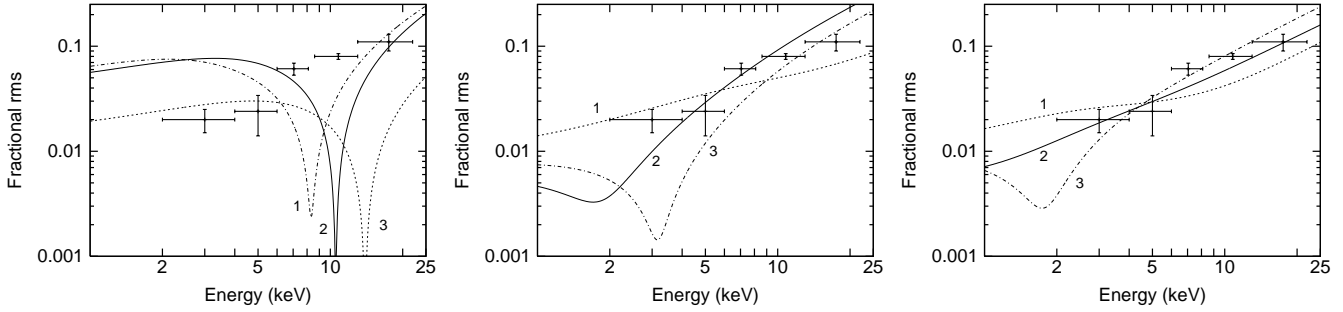


Figure 5. Fractional rms versus energy for the upper kHz QPO (~ 1050 Hz) of 4U 1608-52. The first three low energy data points are taken from the observations on 3-March-1996 and rest high energy data points are the values obtained by averaging over many observations when the upper kHz QPO has a frequency ~ 1000 Hz. The left panel is for the case when the primary driver is in the seed photon temperature. The curves are for different time-averaged spectral models and sizes. Curves 1 and 2 are for the cold seed photon models with $L = 2$ and 1 km respectively. Curve 3 is for the hot seed photon model with $L = 1$ km. The middle and right panels correspond to the case when the primary oscillation is in the medium temperature. The middle panel is for the hot-seed model with $L = 0.5$ km and the curves marked 1, 2, and 3 are for $\eta = 0.65$ ($=\eta_{max}$), 0.4 , and 0.3 respectively. The right panel is for the cold-seed model with $L = 2.0$ km and the curve marked 1, 2, and 3 are for $\eta = 0.47$ ($=\eta_{max}$), 0.3 , and 0.15 respectively. Note that only for the cases considered in the left panel, the associated time-lags will be hard and for the others it would be soft

right panels of Figure 5) explains the qualitative nature of the observed curve with perhaps the cold seed photon model being more favourable.

While, the energy dependent r.m.s of the upper kHz QPO suggests that the primary driver is the coronal temperature, the time-lag suggests otherwise. This is a fairly serious problem for the model, however as we discuss later in the last section, it will be prudent to get better and more concrete evidence that the time-lags are indeed hard, before alternate ideas are explored.

5 The Comptonizing medium width & the kHz QPOs in 4U 1608-52

Like other, NS LMXBs, 4U 1608-52 shows a wide range of kHz QPOs frequencies $\sim 400 - \sim 1200$ Hz. Unfortunately, unlike the March 3rd observation described in the previous section, there are no other reported observations with similar high quality. Using the *RXTE* observations of the 1998 outburst of 4U 1608-52, Barret (2013) found several observations which have kHz QPOs between ~ 560 and ~ 810 Hz. For some of these they measured the time-lag between two broad energy bands (e.g. 3-8 and 8-20 keV) In this work, we refer to these values as mean lags. We have chosen 9 observations from their data for which the observed average kHz QPO frequencies ranged from 580 to 850 Hz. For each observation, we fit the spectrum, as described in §3, using both the hot-seed and cold-seed spectral models. The observations IDs and the corresponding kHz QPO frequency along with thermal Comptonization spectral parameters are listed in Table 1. The total r.m.s. in the energy band 2-60 keV for these lower kHz QPOs have been measured by Mendez, van der Klis, & Ford (2001). The mean soft lag, total r.m.s. and η_{max} for each kHz QPO are listed in Table 2. Here, η_{max} , for both hot & cold-seed spectral models, is computed using Eqn [4].

We now attempt to constrain the medium size and η for each of these observations. Since only the mean time-lag is available, we use the following procedure. We compute the expected mean time lag as function of η for different size or widths of the medium. As an example, the right panel of Figure 6, shows the result of this computation for the observation corresponding to a kHz frequency of 810 Hz using the hot seed photon spectral parameters. The mean

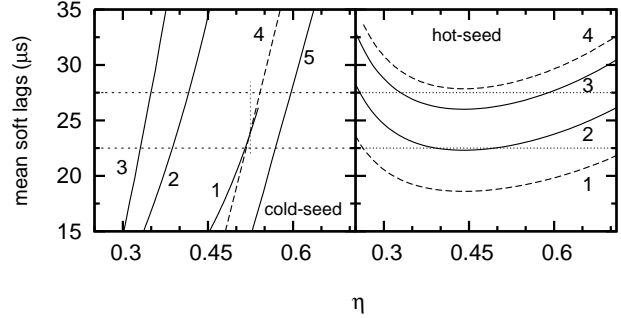


Figure 6. The computed mean soft lags as a function of η at a given size L . The left panel is for the cold-seed photon model and the curves 1, 2, 3, 4, and 5 are for $L = 0.6, 1.5, 5, 11,$ and 12 km respectively. The right panel is for the hot-seed photon models and the curves 1, 2, 3, and 4 are for $L = 0.5, 0.6, 0.7,$ and 0.75 km respectively. The dashed horizontal lines mark the observed range of mean soft lag.

time lag as a function of η is a non-monotonic curve with a minimum and the lags increase with increasing size. The two dashed horizontal lines represent the range of the observed mean time lag and from the Figure, we can estimate the range of η and width for which the curves lies within this range. For the cold seed photon model parameters, the behaviour is more complex. The computed mean time lag increases with η monotonically as shown in the left panel of Figure 6. However, the variation with width is non monotonous with the mean time lag increasing and then decreasing as is evident from the curves marked 1 to 5. In this case, as well we can obtain a range of width and η by considering only values of η smaller than the maximum allowed. We follow the same procedure for the other eight observations and obtain ranges of values for η and width which are plotted in Figure 7. The consolidated results of this analysis are shown in Figure 8 where in the left and middle panels, the estimated range of sizes are plotted versus the QPO frequency and the right panel shows the overlapped allowed ranges for η and size for all nine observations. The primary results of this analysis is that for the hot seed photon model, the size of the Comptonizing medium seems to decrease with increasing QPO frequency while for the cold seed photon model, no such trend is seen, probably because the inferred size ranges are large.

Table 1. The observation IDs, the date, the frequency range and the spectral parameters for nine observations of 4U 1608-52.

ObsID	Start date/time	Freq* (Hz)	Freq (Hz)	Hot-seed-photon model			Cold-seed-photon model		
				kT_b	kT_e	τ^2	kT_b	kT_e	τ^2
10072-05-01-00	1996/03/03	840–890	850	$1.02^{+0.10}_{-0.10}$	$2.69^{+0.04}_{-0.03}$	$38.81^{+2.08}_{-2.02}$	$0.40^{+0.10}_{-0.40}$	$2.6^{+0.09}_{-0.06}$	$40.47^{+3.72}_{-4.48}$
30062-02-01-000	1998/03/24-17:06:23	796-819	810	$1.23^{+0.06}_{-0.06}$	$2.92^{+0.11}_{-0.08}$	$25.87^{+2.75}_{-3.03}$	$0.36^{+0.10}_{-0.31}$	$3.13^{+0.36}_{-0.24}$	$24.33^{+5.72}_{-5.68}$
30062-01-01-00	1998/03/27-15:29:21	752-795	770	$1.28^{+0.04}_{-0.04}$	$3.37^{+0.18}_{-0.14}$	$15.66^{+2.15}_{-2.17}$	$0.34^{+0.09}_{-0.23}$	$4.10^{+0.82}_{-0.61}$	$13.72^{+5.30}_{-5.14}$
30062-01-01-00	1998/03/27-13:53:23	723-750	740	$1.28^{+0.04}_{-0.04}$	$4.28^{+0.59}_{-0.39}$	$9.03^{+2.44}_{-2.37}$	$0.35^{+0.07}_{-0.28}$	$4.87^{+1.11}_{-0.64}$	$10.46^{+3.18}_{-3.17}$
30062-01-01-00	1998/03/27-12:27:36	708-743	710	$1.31^{+0.03}_{-0.03}$	$4.65^{+0.92}_{-0.50}$	$7.89^{+2.43}_{-2.66}$	$0.34^{+0.07}_{-0.29}$	$5.98^{+3.47}_{-1.15}$	$7.70^{+3.54}_{-4.22}$
30062-01-01-02	1998/03/29-10:41:15	661-697	680	$1.20^{+0.02}_{-0.02}$	5.00^J	$7.83^{+0.12}_{-0.12}$	$0.34^{+0.07}_{-0.33}$	$5.54^{+2.86}_{-1.05}$	$9.56^{+4.24}_{-4.86}$
30062-02-01-00	1998/03/24-22:01:31	643-667	650	$1.26^{+0.03}_{-0.03}$	$4.41^{+0.29}_{-0.23}$	$10.04^{+1.35}_{-1.40}$	$0.35^{+0.08}_{-0.34}$	$4.68^{+0.77}_{-0.49}$	$12.23^{+2.91}_{-2.99}$
30062-02-01-01	1998/03/25-18:42:22	595-631	615	$1.23^{+0.03}_{-0.03}$	$5.96^{+0.96}_{-0.69}$	$6.32^{+1.87}_{-1.67}$	$0.33^{+0.07}_{-0.26}$	$6.49^{+5.56}_{-1.59}$	$7.8^{+4.72}_{-6.34}$
30062-02-01-01	1998/03/25-17:46:60	567-576	580	$1.17^{+0.04}_{-0.03}$	$7.25^{+3.98}_{-1.05}$	$5.08^{+1.80}_{-2.95}$	$0.34^{+0.06}_{-0.33}$	$6.40^{+1.28}_{-0.75}$	$8.6^{+2.03}_{-2.26}$

Note: Freq* is the observed frequency range for the observation while Freq is the frequency used to compute time-lags. kT_b is the seed photon source temperature, kT_e the temperature of the Comptonizing medium, and τ is its optical depth. Here τ is different from τ_o of COMPTT and it is calculated by the relation $\tau^2 + \tau = \frac{12}{\pi^2} (\tau_o + 2/3)^2$. The observed QPO frequency range and the spectral parameters for the hot-seed-photon model are taken from Barret (2013) (and reference within).

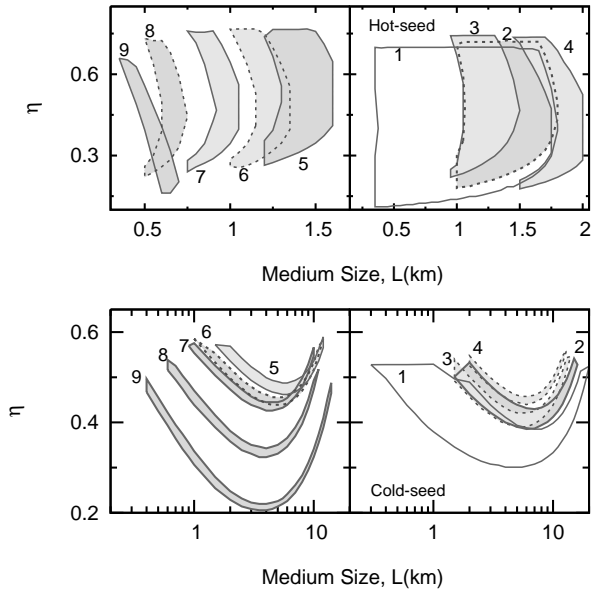


Figure 7. The computed allowed ranges of η and medium size, L . The upper panels correspond to the hot seed photon model while the lower ones correspond to the cold seed photon one. The closed curves 9, 8, 7, 6, 5, 4, 3, 2, and 1 are for lower kHz QPO frequencies of 850, 810, 770, 740, 710, 680, 650, 615, and 580 Hz respectively.

6 SUMMARY AND DISCUSSION

In Paper I, we had shown that the observed soft lags of the lower kHz QPO of neutron star systems, can be explained within the framework of a thermal Comptonization model. Soft lags are expected if the driving oscillation causes variation in the temperature of the medium and if a certain fraction of the photons impinge back to the soft photon source. Apart from identifying the radiative process for the oscillation, the model also holds the promise to give an estimate for the size and geometry of the Comptonizing medium.

In this work, we study the dependence of the results on the model used to represent the time averaged spectrum during the oscillation. In the 3-20 keV spectral band of the RXTE’s PCA, low mass X-ray binaries usually allow for two spectrally degenerate models which are termed as the “hot” and “cold” seed photon model. We also study the possible variation of the size of the

Table 2. The measured mean soft lag (soft lags between (3–8) and (8–30) keV photons), the total r.m.s. (in 2–60 keV) and the calculated η_{max} for the observations listed in Table 1

Freq (Hz)	Mean soft lag (μs)	Total rms (%)	η_{max}^1	η_{max}^2
850	20.5 ± 2.0	7.5 ± 0.5	0.655	0.476
810	25.0 ± 2.5	8.1 ± 0.5	0.728	0.525
770	30.0 ± 2.5	8.3 ± 0.7	0.759	0.569
740	30.0 ± 2.5	9.15 ± 0.65	0.767	0.581
710	34.0 ± 4.0	9.2 ± 0.8	0.766	0.587
680	39.0 ± 3.0	9.5 ± 0.7	0.737	0.555
650	31.0 ± 5.0	8.8 ± 1.0	0.740	0.553
615	28.0 ± 7.0	7.6 ± 0.6	0.724	0.548
580	18.0 ± 12.0	6.3 ± 0.9	0.700	0.528

Note: The data points for the mean soft lags are taken from Barret (2013) and for the total r.m.s. from Mendez, van der Klis, & Ford (2001). The superscript 1 and 2 are for when η_{max} is computed for the hot-seed and cold seed models.

medium as a function of the QPO frequency and attempt to extend the model to data from the upper kHz QPO.

The 3rd March 1996 observation of 4U1608-52 provides one of the best quality time-lag versus energy data for the lower kHz QPO. We compare the model predictions for both the hot and cold seed photon spectral models. We find that qualitatively, for both these spectral shapes, the Comptonization model can explain the r.m.s and time lag as a function of energy. However, the range of the medium size inferred from the hot seed photon model, 0.25-1.0 kms is different from that of the cold seed photon model, 0.5-10.0 kms. Both interpretations require a significant fraction of the photons to impinge back into the soft source with $\eta > 0.2$. While other observations of 4U1608-52 are not of the same high quality as the 3rd March 1996 observations, Barret (2013) have measured for some of them lag between two broad energy bands (e.g. 3-8 and 8-20 keV). For nine such observations corresponding to different QPO frequencies we have attempted to estimate the medium size using both the hot and cold seed photon time-averaged spectral models. For the hot seed photon model, the size of the medium is found to decrease with increasing QPO frequency, while no such trend can be inferred for the cold seed photon model case, probably because here the allowed range for the sizes are larger.

These results show that while it is promising to obtain the size

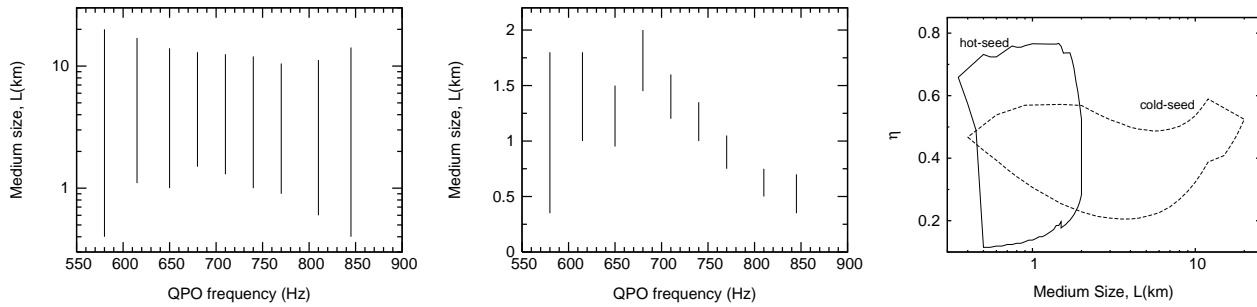


Figure 8. The estimated range of size, L for the nine lower kHz QPO frequency. The left panel is for the cold-seed photon model while the middle is for the hot-seed photon one. The right panel represents the allowed region of η and L by overlapping the regions for each individual frequencies shown in Figure 7.

and geometry of the Comptonizing corona by modelling the energy dependent time-lags, an accurate non-degenerate spectral model for the time-averaged spectrum is critical for such an analysis. Unfortunately, the 3-20 keV energy band of the RXTE PCA does not seem to be sufficient to do this. What is required is a wider band spectral coverage combined with high frequency timing capabilities. The recently launched satellite *ASTROSAT*¹ (Agrawal 2006; Singh et al. 2014) will provide such a unique opportunity, since while the *Large Area X-ray Proportional counters (LAXPC)* will provide high frequency timing capability and spectra in the 3-80 keV band, the *soft X-ray telescope (SXT)* will provide the much needed simultaneous low energy spectra in the 0.3-8 keV band.

During the 3rd March observation of 4U1608-52, an upper kHz QPO (~ 1050 Hz) was also observed and its fractional r.m.s versus energy is similar to the lower kHz one. Indeed, modelling the r.m.s variation requires that the primary driver is the medium temperature variation similar to the lower kHz QPO. However, this implies that for this QPO as well the time-lag should be soft, which seems to be in contradiction with the results obtained by de Avellar et al. (2013) where they measure the time lag for the upper kHz QPO to be hard. While the significance of the lag detection is less than that of the lower kHz QPO, this is a challenge to the simple Comptonization model presented here. This may indicate that reverberation lags due to time delays between a primary and its reflected spectrum maybe dominant. While it seems unlikely that these reverberation lags can explain the entire energy behaviour of the lower kHz QPO (Cackett 2016), a combination of Comptonization and reverberation lags maybe possible. It could also be that the time averaged spectra of these sources are more complex than assumed here and perhaps the dominant Comptonization component is not a single temperature one but instead forms from multiple zones. Such complexities in the spectra including the presence of dominant reflection components, would require broad band sensitive instruments.

Soft lags within the thermal Comptonization framework require that a significant fraction of the photons impinge back to the soft photon source which as demonstrated in this work, can be broadly constrained. This naturally puts restrictions on the geometry of the system. For example, if the Comptonizing medium is a thin shell around the soft photon generating neutron star surface, the fraction is expected to be large compared to a geometry where the medium is hot torus like disk surrounded by a soft photon generating accretion disk. The fraction of the photons impinging back into the soft photon source can be estimated for a particular ge-

ometry using a Monte Carlo code to simulate the Comptonization process. Thus, in a near future work, we plan to develop and use such a Monte Carlo code to understand what kind of geometry is allowed.

ACKNOWLEDGEMENTS

NK thanks CSIR/UGC for providing support for this work.

References

- Agrawal P. C., 2006, *Advances in Space Research*, 38, 2989
 Agrawal, V.K., Sreekumar P., 2003, *MNRAS*, 346, 933
 Agrawal, V.K., Misra R., 2009, *MNRAS*, 398, 1352
 Altamirano, D., van der Klis, M., Mendez, M., Jonker, P.G., Klein-Wolt, M., Lewin, W.H.G., 2008, *ApJ*, 685, 436
 Barret, D., 2001, *Adv. Space Res.*, 28, 307
 Barret, D., 2013, *ApJ*, 770, 9
 Belloni, T., Mendez, M., Homan, J., 2005, *A&A*, 437, 209
 Belloni, T., Mendez, M., Homan, J., 2007, *MNRAS*, 376, 1133
 Berger, M., van der Klis, M., van Paradijs, J., Lewin, W.H.G., Lamb, F., Vaughan, B., Kuulkers, E., Augusteijn, T., Zhang, W., Marshall, F.E., Swank, J.H., Lapidus, I., Lochner, J.C., Strohmayer, T.E., 1996, *ApJ*, 469, L13
 Cabanac, C., Henri, G., Petrucci, P.-O., Malzac, J., Ferreira, J., Belloni, T.M., 2010, *MNRAS*, 404, 738
 Cackett E. M., 2016, arXiv, arXiv:1601.07849
 de Avellar, M.G.B., Mendez, M., Sanna, A., Horvath, J.E., 2013, *MNRAS*, 433, 3453
 Di Salvo, T., Stella, L., 2002, in *Proc. of the XXII Moriond Astrophysics Meeting, The Gamma-Ray Universe*, ed. A. Goldwurm, D. Neumann, & J. Tran Thanh Van, 67; arXiv:astro-ph/0207219v1
 Erkut, M.H., Psaltis, D., Alpar, M.A., 2008, *ApJ*, 687, 1220
 Farinelli, R., Titarchuk, L., Frontera, F., 2007, *ApJ*, 662, 1167
 Farinelli, R., Titarchuk, L., Paizis, A., Frontera, F., 2008, *ApJ*, 680, 602
 Ford E.C., van der Klis, M., Mendez, M., Wijnands, R., Homan, J., Jonker, P.G., van Paradijs, J., 2000, *ApJ*, 537, 368
 Gierlinski, M., Done, C., 2002, *MNRAS*, 337, 1373
 Gierlinski, M., Zdziarski, A.A., 2005, *MNRAS*, 363, 1349
 Hasinger, G., van der Klis, M., 1989, *A&A*, 225, 79
 Homan, J., van der Klis, M., Fridriksson, J.K., Remillard, R.A., Wijnands, R., Mendez, M., Lin, D., Altamirano, D., Casella, P., Belloni, T.M., Lewin, W.H.G., 2010, *ApJ*, 719, 201

¹ <http://astrosat.iucaa.in>

- Kaaret, P., Piraino, S., Ford, E.C., Santangelo, A., 1999, *ApJ*, 514, L31
- Kato, S., 2009, *PASJ*, 61, 1237
- Kluźniak, W., Abramowicz, M.A., 2001, *astro-ph/0105057*
- Kompaneets, A. S. 1957, *Soviet Phys. JETP*, 4, 730
- Kumar, N., Misra, R., 2014, *MNRAS*, 445, 2818 (Paper I)
- Lamb, F.K., Miller, M.C., 2003, *astro-ph/0308179*, 10pp.
- Lee, H.C., Miller, G.S., 1998, *MNRAS*, 299, 479
- Lee, H.C., Misra, R., Taam, R.E., 2001, *ApJ*, 549, L229
- Li, X.-D., Zhang, C.-M., 2005, *ApJ*, 635, L57
- Lin, D., Remillard, R.A., Homan, J., 2007, *ApJ*, 667, 1073
- Lin, D., Remillard, R.A., Homan, J., 2009, *ApJ*, 696, 1257
- Lin, Y.-G., Boutelier, M., Barret, D., Zhang, S.-N., 2011, *ApJ*, 726, 74
- Lin, D., Remillard, R.A., Homan, J., Barret, D., 2012, *ApJ*, 756, 34
- Mendez, M., van der Klis, M., van Paradijs, J., Lewin, W.H.Z., Vaughan, B.A., Kuulkers, E., Zhang, W., Lamb, F.K., Psaltis, D., 1998a, *ApJ*, 494, L65
- Mendez, M., van der Klis, M., Wijnands, R., Ford, E.C., van Paradijs, J., Vaughan, B.A., 1998b, *ApJ*, 505, L23
- Mendez, M., van der Klis, M., Ford, E.C., Wijnands, R., van Paradijs, J., 1999, 511, L49
- Mendez, M., van der Klis, M., 1999, *ApJ*, 517, L51
- Mendez, M., van der Klis, M., Ford, E.C., 2001, *ApJ*, 561, 1016
- Miller, M.C., Lamb, F.K., Psaltis, D., 1998, *ApJ*, 508, 791
- Misra R., Shanthi K., 2004, *MNRAS*, 354, 945
- Mitsuda K., et al., 1984, *PASJ*, 36, 741
- Mitsuda K., Inoue H., Nakamura N., Tanaka Y., 1989, *PASJ*, 41, 97
- Mukherjee A., Bhattacharyya S., 2012, *ApJ*, 756, 55
- Mukhopadhyay, B., 2009, *ApJ*, 694, 387
- Osheroich, V., Titarchuk, L., 1999, *ApJ*, 522, L113
- Paizis A., Ebisawa, K., Tikkanen, T., Rodriguez J., Chenevez, J., Kuulkers, E., Vilhu O., Courvoisier T. J.-L., 2005, *A&A*, 443, 599
- Paizis A., Farinelli R., Titarchuk L., Courvoisier T. J.-L., Bazzano A., Beckmann V., Frontera F., Goldoni P., Kuulkers E., Mereghetti S., Rodriguez J., Vilhu O., 2006, *A&A*, 459, 187
- Pal, P.S., Chakrabarti, S.K., 2014, *MNRAS*, 440, 672
- Peille P., Barret D., Uttley P., 2015, *ApJ*, 811, 109
- Psaltis, D., 2006, *Compact Stellar X-ray Sources*, Chept. 1, eds. Lewin, W.H.G., and van der Klis, M. (Cambridge Astrophysics Series 39)
- Raichur H., Misra R., Dewangan G., 2011, *MNRAS*, 416, 637
- Sanna, A., Mendez, M., Belloni, T., Altamirano, D., 2012, *MNRAS*, 424, 2936
- Shi, C., Li, X.-D., 2009, *MNRAS*, 392, 264
- Singh K. P., et al., 2014, in *Society of Photo-Optical Instrumentation Engineers (SPIE) Conference Series 9144*, 1
- Stella, L., Vietri, M., 1999, *Phys. Rev. Lett.*, 82, 17
- Straaten, S., van der Klis, M., Mendez, M., 2003, *ApJ*, 596, 1155
- Tarana, A., Bazzano, A., Ubertini, P., 2008, *ApJ*, 688, 1295
- Titarchuk, L., 2003, *ApJ*, 591, 354
- van der Klis, M. 2000, *ARA&A*, 38, 717
- van der Klis, M., 2006, *Compact Stellar X-ray Sources*, Chept. 2, eds. Lewin, W.H.G., and van der Klis, M. (Cambridge Astrophysics Series 39)
- Vaughan, B.A., van der Klis, M., Mendez, M., van Paradijs, J., Wijnands, R.A.D., Lewin, W.H.G., Lamb, F.K., Psaltis, D., Kuulkers, E., Oosterbroek, T., 1997, *ApJ*, 483, L115; erratum 509, L145 (1998)
- Wang, D.H., Chen, L., Zhang, C.M., Lei, Y.J., Qu, J.L., 2013, *MNRAS*, 435, 3494
- White N. E., et al., 1986, *MNRAS*, 218, 129
- Wijnands, R.A.D., van der Klis, M., van Paradijs, J., Lewin, W.H.G., Lamb, F.K., Vaughan, B., Kuulkers, E., 1997, *ApJ*, 479, L141
- Wijnands, R., Homan, J., van der Klis, M., Mendez, M., Kuulkers, E., van Paradijs, J., Lewin, W.H.G., Lamb, F.K., Psaltis, D., Vaughan, B., 1997, *ApJ*, 490, L157
- Yu, W., Zhang, S.N., Harmon, B.A., Paciesas, W.S., Robinson, C.R., Grindlay, J.E., Bloser, P., Barret, D., Ford, E.C., Tavani, M., Kaaret, P., 1997, *ApJ*, 490, L153
- Zhang, W., Lapidus, I., White, N.E., Titarchuk, L., 1996, *ApJ*, 469, L17
- Zhang, C., 2004, *A&A*, 423, 401